Progress In Electromagnetics Research M, Vol. 110, 109–118, 2022

Pre-Compliance Near-Field Tests Based on Oscilloscopes

Marcelo B. Perotoni[1, *], Walter M. Silva[1], Danilo B. Almeida[2], and Kenedy M. G. Santos[2]

Abstract—This paper covers the use of oscilloscopes in near-field, pre-compliance radiating tests. Using commercial low-cost planar magnetic probes, a procedure is presented to use the time-domain waveforms to address emitted radiation patterns. In spite of its lower sensitivity in relation to spectrum analyzers, a comparison between the two instruments is presented, with the inferior response of the oscilloscope compensated by means of off-the-shelf broadband amplifiers. Complete system calibration is described and performed, relating the voltage measurements in a transmission-line structure to field amplitudes provided by a full-wave simulation. Two different typical devices are tested using the procedure here developed: a direct current motor, driven by a square wave, and a microprocessor board. Results show the potential use of the almost omnipresent instrument in sophisticated field evaluations, enabling its use in situations where spectrum analyzers are not available.

1. INTRODUCTION

Pre-compliance procedures are relevant, particularly during early design stages involving electronic products. Though the exact pre-compliance definition is somewhat blurred, it can be understood as evaluations provided by unaccredited laboratories. The lack of accreditation does not allow official statements or certifications with regard to the measured product or system, since compliance standards are not fully obliged. Moreover, depending on the enterprise size or its output volume, a full-compliance laboratory might not be cost-effective. Therefore, low-cost methods that address radiation or immunity issues are well known within EMC (electromagnetic compatibility), providing means to not only detect design flaws but also quickly troubleshoot defective prototypes. Interesting guidelines for low-cost pre-compliance techniques and instruments are found in [1, 2].

Spectrum analyzers (SA) are many times absent in hardware development laboratories, and it is usually the most expensive item in a pre-compliance laboratory [1], with oscilloscopes still being the workhorse tool of analog and digital design. For instance, a pre-compliance CISPR-16 EMC conducted emission test had a sampling oscilloscope employed with success [3]. For this specific case, the lower sensitivity of the instrument in contrast to SA was not an issue, due to higher levels captured in conducted tests. In [4], a custom-made ultra-wideband amplifier was used to increase the signal level, for radiating tests. In case a frequency domain analysis is needed, built-in FFT (Fast-Fourier Transform) routines in the oscilloscope can be used to narrow down emissions or determine other frequency domain visualizations. Besides its popularity, oscilloscopes have an inherent broadband behavior, capturing with a flat-amplitude response, waveforms from DC (direct current) up to their frequency limit. In contrast to SAs, which do not display signals after their upper limit, samples beyond the oscilloscope maximum frequency are still shown, in spite of being beyond the flat response region. In practice, these beyond-the-limit voltage amplitudes might not be correctly displayed.

Received 25 March 2022, Accepted 26 April 2022, Scheduled 7 May 2022
* Corresponding author: Marcelo Bender Perotoni (marcelo.perotoni@ufabc.edu.br).
[1] UFABC, Brazil. [2] IFBA, Brazil.

Particularly with EMI (electromagnetic interference) applications, bursts and intermittent emissions are tricky to be captured by frequency-domain instrumentation, since the desired bandwidth is sequentially swept and might not be fast enough. Oscilloscopes, in turn, acquire the time-domain samples all at once, favoring the transients acquisition. In order to cover burst-type emissions, FFT Spectrum Analyzers use fast analog-to-digital converters to save the entire waveform in memory and later perform the mathematical operation, so that there is no need to perform a sweep oscillation across the band. Therefore, FFT SAs are able to capture burst emissions, though at higher costs.

Within the pre-compliance arsenal, near-field (NF) probes are very useful to pinpoint the possible causes of emitters in complex electronic boards or systems [5], even within confined volumes [6]. A more sophisticated application of NF scanning is the substitution of EMI emitters by equivalent sources (dipoles or loops). Accurate computer modeling of complex and multi-layered printed-circuit boards is still daunting [4], as well as scenarios with many details whose characteristics and geometries are not well defined, such as harnesses and electric motors inside vehicle chassis. Therefore, the substitution of complex sources by an equivalent mathematical counterpart enables a much more efficient modeling and further analyses [7]. However, these substitutions depend on complex quantities, which are not provided by scalar SAs unless specific arrangements are employed. Using two channels of an oscilloscope, however, one fixed as a reference and the other spatially sweeping the device under test, relative phases can be extracted. A higher-end alternative to both oscilloscope and SA, the vector network analyzer, provides the needed complex information, due to their coherent reception. Sundry details concerning the phase information on field measurements using instrumentation are discussed elsewhere [8].

This article reports the use of oscilloscopes in NF measurements using magnetic probes, moved by an automatic 3D positioning matrix. A practical assessment of the sensitivity difference of both oscilloscope and spectrum analyzer is provided, and also the calibration for two low-cost magnetic NF probes. Two devices are measured with the system; a DC motor and a microprocessor board, to illustrate the process.

2. SENSITIVITY COMPARISON

Most modern oscilloscopes offer an FFT operation based on digitally stored waveforms, in contrast to purely analog counterparts. So, in practice, the users may have the impression that they can replace spectrum analyzers. However, some differences arise when internal block diagrams are taken into account. Oscilloscopes have a broadband input frontend, which allows noise to come in through the whole band, whereas SAs electronic filters and average routines decrease the noise influence. In order to reduce the large noise energy, postprocessing can be used in the acquired oscilloscope data so that the band of interest can be digitally separated. SAs can also have their sweep time and resolution bandwidth adjusted, thereby increasing the minimum detectable amplitude level, an operation not possible in oscilloscopes.

Another important figure of merit is the dynamic range, i.e., the amplitude between the largest and faintest measured signals. While the former is defined by the instrument sensitivity and is influenced by its input bandwidth and also depends on the number of bits that the analog-to-digital converter operates; the latter depends on the influence of secondary products due to large amplitude incoming signals. SAs have, overall, a much larger dynamic range, typically 90 dB, whereas oscilloscopes operate around 50 dB.

In EMC and general radiofrequency applications, a subtle issue that arises when the two instruments are compared is their input impedance. Spectrum analyzers have standard 50 Ω or 75 Ω inputs, in contrast to 100 MΩ high-impedance oscilloscope probes. The main idea in SAs is the minimization of reflections loss while oscilloscopes aim at reduced loading influence on the circuit under test, approaching an open-circuit condition. When dealing with systems showing transmission lines effects, namely mismatches and reflections, oscilloscopes measurements should consider this frequency-dependent loss.

For the sake of comparison, a procedure (Fig. 1) was devised to show a quantitative sensitivity analysis. A Rohde & Schwarz FS315 spectrum analyzer was directly connected to a signal generator, whose amplitude was adjusted to be 10 dB above the noise floor. To keep the same reference impedance, a 50 Ω resistor loads the signal generator connected to the Agilent InfiniiVision DSO-X 2024A oscilloscope, but in this case, the test signal was set to on-off keying, to ease the visualization. The amplitude level

on the generator was increased until met the condition $V_{\text{signal}} = 3.16 \cdot V_{\text{noise}}$, equivalent to the 10 dB in power.

The signal generator was swept up to 200 MHz, chosen because it is the maximum frequency of the oscilloscope. SA bandwidth was kept at the same 200 MHz, the exception of frequencies below 1 MHz, due to low-frequency leaking in the instrument. Therefore, it was used a maximum frequency of 10 MHz (discrete points at 1 MHz and 500 kHz) and 500 kHz (at 100 kHz and 10 kHz). Results in Fig. 1 show that the spectrum analyzer noise floor is at least 10 dB lower than that from the oscilloscope, proving its higher sensitivity. No filtering of averaging was employed throughout the test, to keep the data as raw as possible.

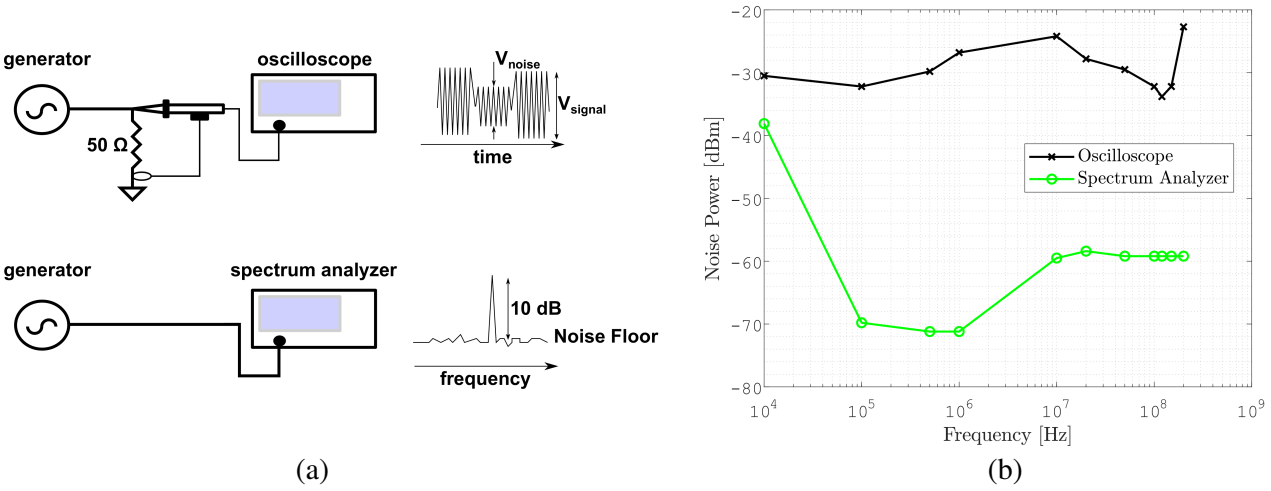

Figure 1. Block diagram of (a) the measurement instruments and (b) their noise floor curve.

3. NEAR-FIELD PROBES AND THEIR CALIBRATION

As the name implies, NF probes are meant to respond to fields emitted in the source vicinity. They can be sensitive to either electric or magnetic fields, in contrast to far-field counterparts (antennas), due to the fact that in the near-field region fields are not coupled, so their nature depends on the source type [5]. Unlike antennas, NF sensors operate close to the equipment under test, therefore there is a perturbation of the existing fields due to their presence, a factor that should be minimized or taken into account using a further analysis, as suggested by [5]. With respect to the electrical size, NF probes are usually very small, whereas antennas have physical dimensions close to $\lambda/2$ [1]. Their small sizes allow spatial sampling of fields close to a circuit under test so that possible causes of emission can be pinpointed (e.g., common-mode currents, radiation from heat dissipators, etc.), offering good spatial resolutions. Unfortunately, there is a trade-off for the case of loops: their sensitivity is proportional to their area, so in the case of poor output levels amplifiers need to be used [9]. Fig. 2 shows examples of commercial probes, two planar loops, and a dipole, used as a comparison. Measurements of their impedance were performed, their S_{11} response is clearly non-resonant, so it helps minimize the electromagnetic coupling with the source. Both loops show a self-resonant frequency within this bandwidth, i.e., 90 MHz for the G loop and 80 MHz for the larger XL loop. In contrast, the dipole input impedance characteristic is capacitive throughout the whole range. Taking advantage of the circuit representation of magnetic field probes, [10] was able to predict the voltages due to both electric and magnetic components, with frequencies in the GHz range.

NF probes provide outputs in terms of voltages (oscilloscopes) or power levels (SAs). Information of the emitted frequency and relative (qualitative) comparisons are usually enough for pre-compliance [1]; however, to retrieve absolute field levels sampled by the probes a conversion is needed, expressed by the

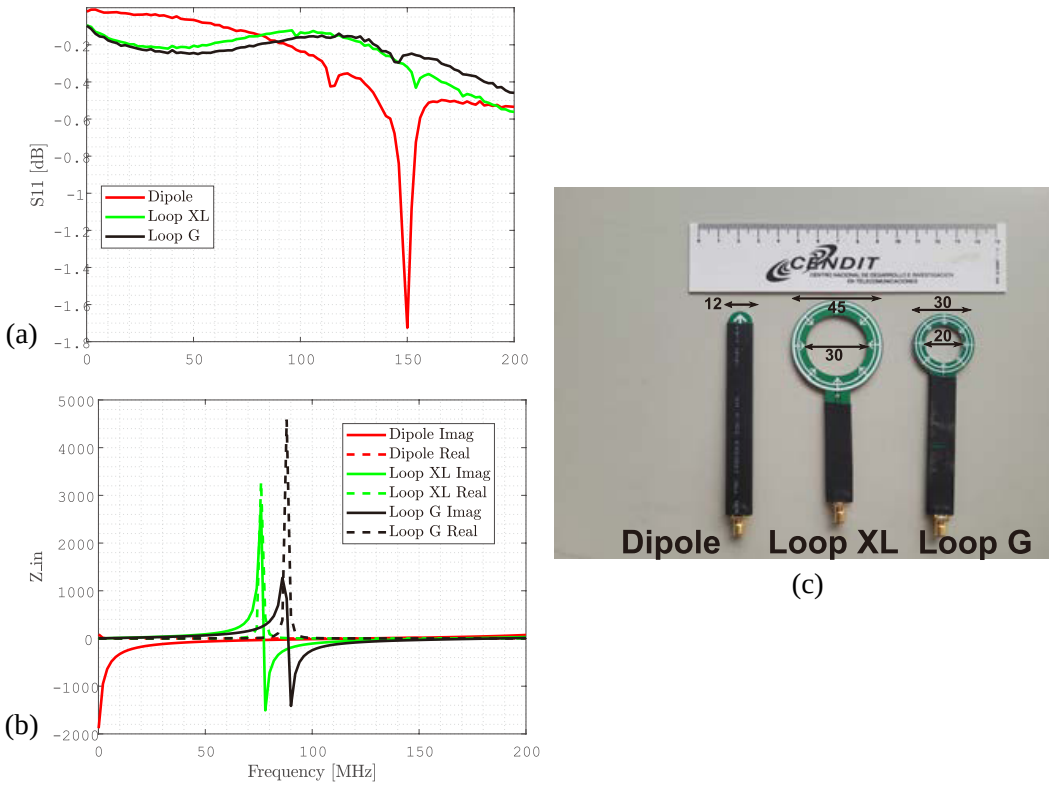

Figure 2. (c) used probes and (a) measured S parameters and (b) input impedance. Dimensions: mm.

AF (Antenna Factor) [11], here considering a magnetic-field type sampling:

$$AF = \frac{H_i}{V_{rec}} \tag{1}$$

where H_i is the magnetic existing field at the probe position, and V_{rec} is the output available voltage. The setup shown in Fig. 3 is used. A transverse electro-magnetic (TEM) structure, with a wire h away from the ground plane generates fields when connected to a signal generator (15 dBm continuous wave), between 10 MHz and 200 MHz. The line is terminated in two 100 Ω parallel resistors. Two types of orthogonal responses are evaluated for the loops: E-response and H-response, the first ideally null in shielded and improved magnetic NF probes [12–14]. However, electrically small loop probes are sensitive only to the magnetic field [9, 15], as long as their radius r follows $2r/\lambda < 0.01$. When applied to the XL and G loops, it imposes a limit to the electrostatic response of 67 MHz and 100 MHz, respectively. Sensitivity to the electric field increases 40 dB per decade, whereas the magnetic field slope is 20 dB per decade, so effects of the field contamination in NF loops increase in higher frequencies [10]. The lower oscilloscope sensitivity required a chain of two broadband amplifiers, resulting in a net 30 dB gain starting from 10 MHz. A similar NF probe using the oscilloscope in time-domain imaging used a custom-designed amplifier and the line excited with 20 V peak-to-peak [4], in contrast to the 3.56 V here employed.

Measured oscilloscope voltages are stored and later analyzed. Field values are obtained from a FEKO model. The setup had the probe placed 10 mm above the middle point of the transmission line. Though the oscilloscope has a maximum bandwidth of 200 MHz, its time-division settings go beyond this limit. For the present calibration, all measured voltages were saved as ascii files, with time division set to 500 ns, resulting in a sampling frequency of 200 MHz. Per default, the instrument saves 2000 samples at once, so to increase frequency resolution 10 sequences were stored in time domain. With respect to the polarization of fields, the H-response was considered to be the magnetic field component orthogonal to the loop plane whereas the E-response was defined to respond to the magnetic component collinear with the same plane.

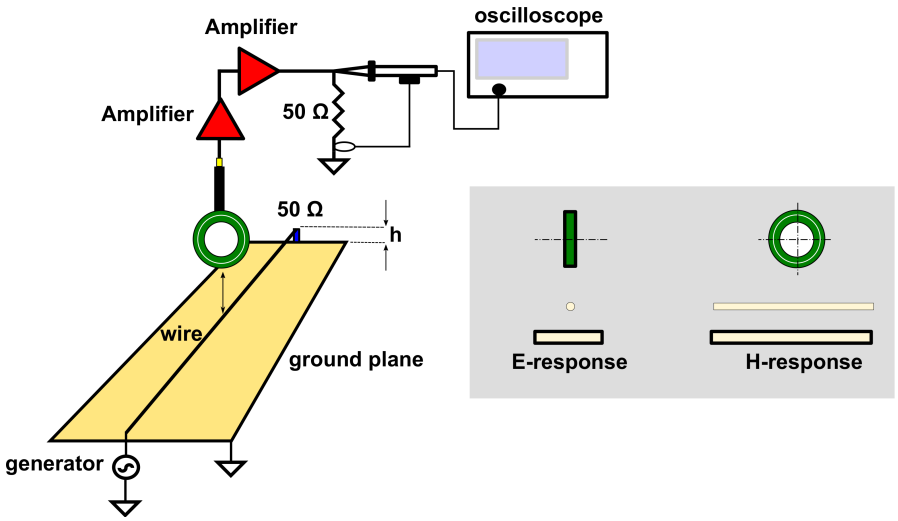

Figure 3. Setup used for addressing the AF measurement. Two different types of excitation are shown on the inset box at right. $h = 9\,\text{mm}$.

Existing noise contaminated the measurements since an unshielded laboratory was used. Raw voltage samples were then digitally filtered (Matlab IIR designfilt function), in order to extract the desired frequency range. The calibration steps can be summarized:

- Set the generator frequency and power level, connected to the TEM line.
- Acquire N vectors of the loop voltage connected to the oscilloscope, with the appropriate distance and orientation in regard to the transmission line.
- Concatenate the N different vectors and (bandpass) filter the sequence to isolate the excited input frequency.
- Extract the final voltage amplitude in the time-domain filtered waveform.
- Compute AF, the ratio between the simulated magnetic field and measured voltage amplitudes.

Figure 4 shows the time and frequency curves, when 10 MHz was applied to the TEM line, along with the ambient noise. Strong interfering signals are seen in the broadcast FM (88 to 108 MHz), and

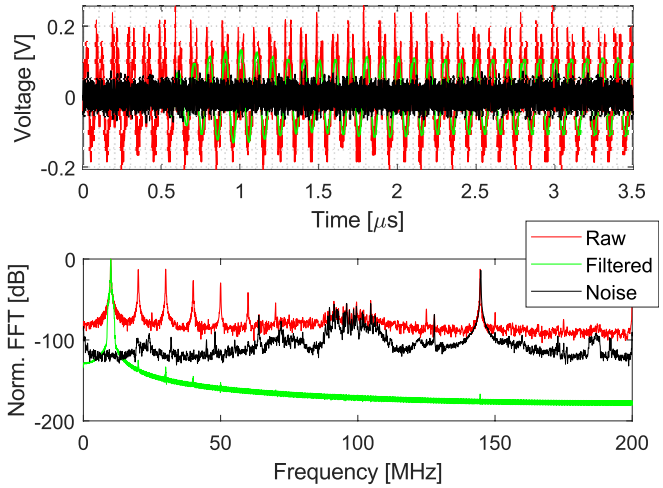

Figure 4. (a) Voltage levels of the XL loop receiving the ambient noise and 10 MHz signal radiated by the TEM line, with and without filtering. (b) Frequency spectra.

close to 150 MHz and 180 MHz. Digital filtering reduced these interfering energies, as seen in the filtered time-domain waveform.

NF probe positioning was ensured by a homemade 3D matrix (1 mm resolution in 3-axes), shown with the final AF results, units in decibels to ease the visualization, in Fig. 5. Though with different sizes, both loops showed similar sensitivities, and the ideally-null response for the E-excitation is found to be approximately 40 dB below the expected H-excitation, in spite of the unshielded probe designs.

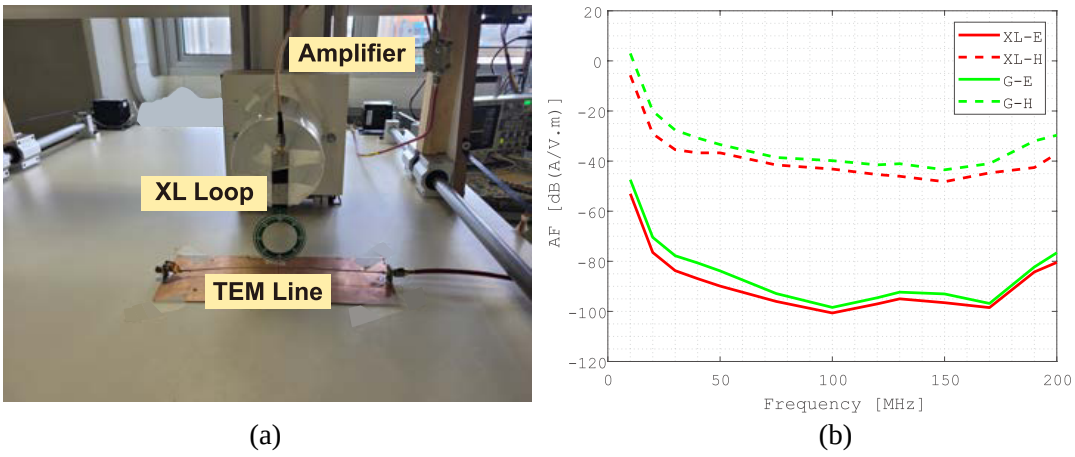

Figure 5. (a) Setup used for calibration and (b) AF curves, for the XL and G loops. E and H cases are defined according to Fig. 3. Only one amplifier is visible, the other one is obstructed by the structure.

Other methods are employed for the calibration, such as analytical formulas describing field amplitudes around TEM lines [16], which can be used to extract the absolute field levels. Another interesting method involves the use of an exciting loop whose current is sampled by a series resistor and using it as input to Ampère law, therefore computing the magnetic field at the probe position [6]. This method is particularly relevant for frequencies where impedance mismatches effects are not important. The rectangular probe, in particular, had closed-form expressions derived for the voltage-to-field conversions [17].

4. APPLICATIONS

4.1. DC Motor

DC motors are usually employed with H-bridge drives allowing electronic speed control and bidirectional rotation. Square waves used in the PWM (pulse-width modulation) signals contain strong harmonic content, several times far away from the fundamental pulse repetition frequency, which might radiate and disturb nearby high-impedance systems. A DC motor behavioral model, intended to be used for automotive radiated and conducted emissions, was developed [18] for frequencies limited to 100 MHz, using the commercial suite EMC Studio. Here, a low-cost DC motor was excited by a 1 MHz square wave (17 ns rise and fall times), 5 V peak-to-peak amplitude, with the emitted signal captured by the XL loop with two broadband amplifiers. Fig. 6 shows the XL loop positioned at the maximum amplitude radiation spot (approximately 1 cm from the contacts), with the time and frequency spectra of both signal and noise. It can be seen that in spite of the 1 MHz frequency, emissions were found to be relevant between 30 and 40 MHz, with the time-domain sequence displaying the emission intermittent and aperiodic characteristics. By optimizing the time-division scale, the signal visualization can be improved, first aiming at long sampling times (here 100 ms), and later adjusting with finer time divisions (used 500 ns) to afford a higher maximum frequency. Similar investigation with SA would require a more complex procedure due to the intermittent emission nature, so this application is well suited to oscilloscope analyses.

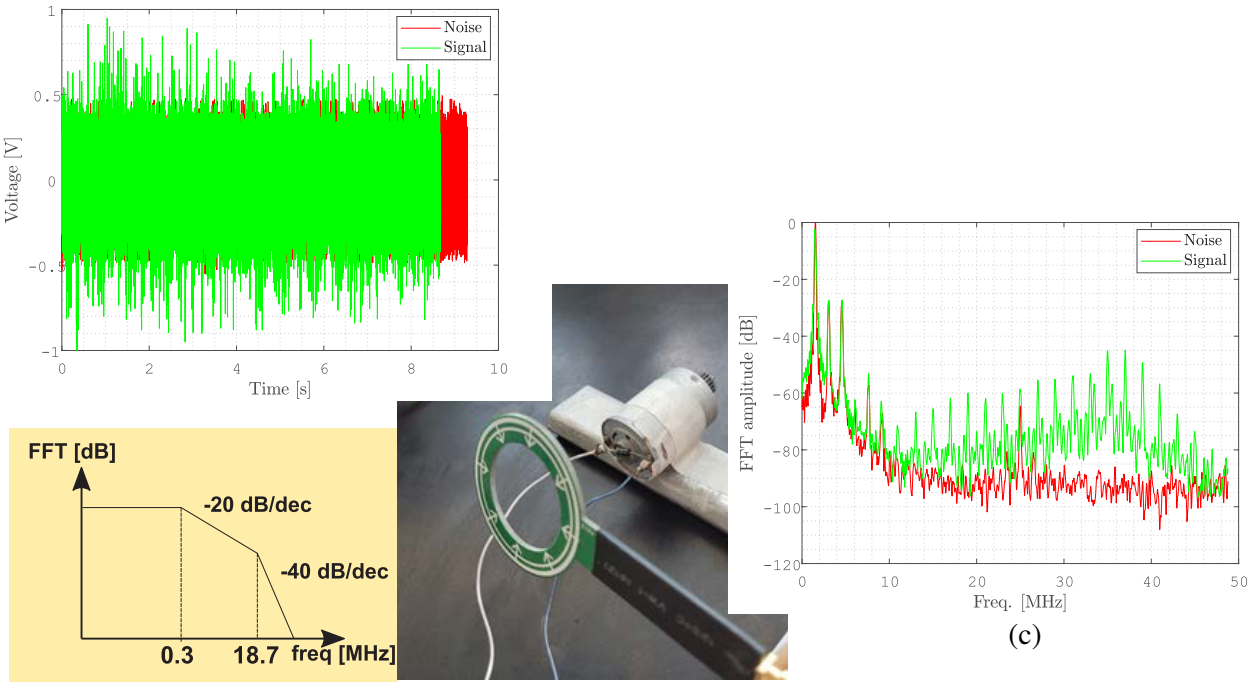

Figure 6. (b) DC motor setup, (a) its time and (c) normalized output frequency spectra. Inset on the left bottom shows the theoretical [11] frequency domain envelope at the input.

4.2. Application: Galileo Board

Galileo is an Arduino-compatible board, introduced in 2014 and discontinued three years later, powered by an Intel Quark X1000 400 MHz processor with several peripherals, such as I/O, USB, and Ethernet. The board was loaded with a script that simply blinked its led diode at a 1 Hz rate. Initially, Fig. 7 contains the broadband spectrum captured by the SA, with blocks separating the oscilloscope bandwidth and the clock fundamental and second harmonics. A large part of the emissions lies in lower frequencies,

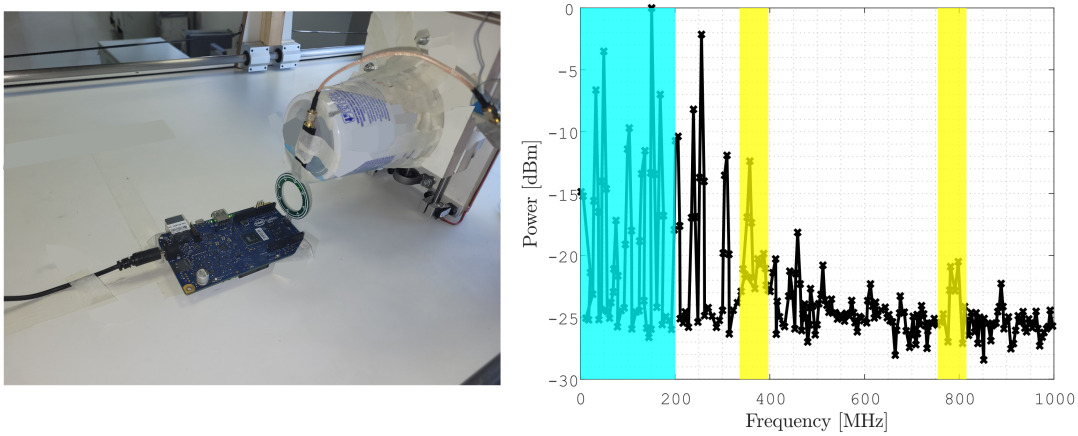

Figure 7. (a) Galileo on the 3D positioning matrix. (b) Broadband emissions; blue box shows the oscilloscope bandwidth and the two yellow bands enclose the clock fundamental and second harmonic.

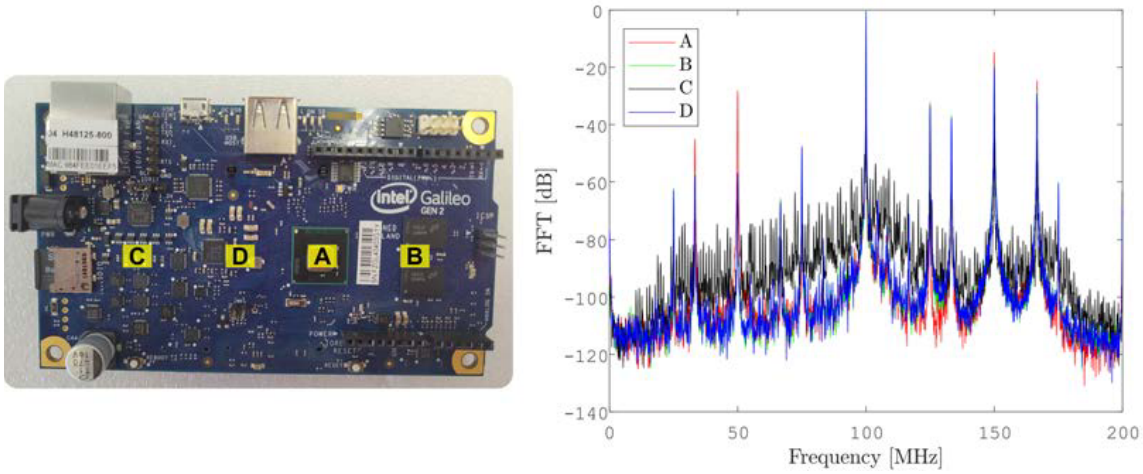

(a) (b)

Figure 8. (a) Galileo board measured points and (b) the normalized captured emissions.

within the oscilloscope range. It also shows the board and XL loop, moved by the 3D matrix. A plastic container physically separated the probes from the moving head, due to its influence on the acquired fields.

Figure 8 depicts the Galileo board and four different measured points, all kept 1 cm above the board. It was found that the microprocessor (point A) is the main emission source, with the signal signature varying as the probe is swept across the board. Results were captured and shown in a normalized format.

Using the computed AF it is possible to estimate magnetic field amplitudes at some maximum points in the frequency domain, results shown in Table 1. To keep the consistency, the same calibration procedure was followed, i.e., filtering the time-domain stored data and later applying the AF conversion factor to the peak voltage, as to retain absolute field values. It can be seen that discrete frequencies of 50 MHz, 150 MHz, and 166.5 MHz generated larger emissions, with the 100 MHz case still suspect to be partly due to contributions from existing nearby FM broadcast energies.

Table 1. Computed magnetic field amplitudes.

Point	Frequency [MHz]	Field amplitude [mA/m]
A	33	1.01
A	50	2.82
D	75	0.53
B	100	4.34
B	125	0.80
B	133	0.50
A	150	1.36
A	166.5	2.02
D	175	0.30

5. CONCLUSION

This article reported the use of oscilloscopes with near-field probes, for EMC pre-compliance radiation tests. In spite of its inferior sensitivity in comparison to costly spectrum analyzers, they can be used to address printed-circuit board emissions with success, as long as certain procedures are followed. The inclusion of external broadband amplifiers increases the sensitivity, and a calibration process can help determine absolute field values picked up by inexpensive near-field probes. Two common devices were tested — a DC motor, excited by a square-wave signal, and a microprocessor board. Results showed the potential of its use in cases where only oscilloscopes are available, taking advantage of their broadband nature, low cost, and post-processing the time-domain data to increase the signal-to-noise ratio.

ACKNOWLEDGMENT

The authors thank the Pro-Rectory for Research, Graduate and Innovation (PRPGI) and the Federal Institute of Education, Science and Technology of Bahia.

REFERENCES

1. Ott, H. W., *Electromagnetic Compatibility Engineering*, Wiley, Hoboken, 2009.
2. Pontt, J., R. Olivares, H. Carrasco, V. Keller, M. López, H. Robles, S. Díaz, A. Toro, and C. Fuentes, "Developing a simple, modern and cost effective system for EMC precompliance measurements of conducted emissions," *2007 European Conference on Power Electronics and Applications*, Aalborg, Denmark, September 2007.
3. Parvis, M., G. Perrone, and A. Vallan, "A precompliance EMC test-set based on a sampling oscilloscope," *IEEE Trans. Instrum. Meas.*, Vol. 54, No. 4, 1220–1223, 2003.
4. Liu, Y. and B. Ravelo, "Fully time-domain scanning of EM near-field radiated by RF circuits," *Progress In Electromagnetics Research B*, Vol. 57, 21–46, 2014.
5. Bienkowski, P. and H. Trzaska, *Electromagnetic Measurements in the Near Field*, Scitech, Raleigh, 2012.
6. Fano, W. G., R. Alonso, and L. M. Carducci, "Near field magnetic probe applied to switching power supply," *IEEE Global Electromagnetic Compatibility Conference (GEMCCON)*, La Plata, Argentina, November 2016.
7. Ramesan, R. and D. Madathil, "Modeling of radiation source using an equivalent dipole moment model," *Progress In Electromagnetics Research B*, Vol. 89, 157–175, 2020.
8. Mynster, A. P. and M. Sørensen, "Validation of EMC near-field scanning amplitude and phase measurement data," *International Symposium on Electromagnetic Compatibility — EMC EUROPE*, Rome, Italy, 2012.
9. Attaran, A., W. Handler, and B. A. Chronik, "2 mm radius loop antenna and linear active balun for near field measurement of magnetic field in MRI-conditional testing of medical devices," *IEEE Trans. Electromagn. Compat.*, Vol. 62, No. 1, 186–193, 2020.
10. Liu, S., X. Fang, T. Song, M.-H. Kim, H.-W. Shim, and C. Hwang, "Field coupling mechanism investigation of mm-Wave magnetic near-field probe based on a generalized equivalent circuit," *IEEE Trans. Instrum. Meas.*, Vol. 71, Art no. 8002409, 1–9, 2022.
11. Paul, C. R., *Introduction to Electromagnetic Compatibility*, Wiley, Hoboken, 2006.
12. Yan, Z., J. Wang, W. Zhang, Y. Wang, and J. Fan, "A simple miniature ultrawideband magnetic field probe design for magnetic near-field measurements," *IEEE Trans. Antennas Propag.*, Vol. 64, No. 12, 5459–5465, 2016.
13. Sivaraman, N., F. Ndagljlmana, M. Kadi, and Z. Riah, "Broad band PCB probes for near field measurements," *2017 International Symposium on Electromagnetic Compatibility — EMC Europe*, Angers, France, September 2017.

14. Bang, J., Y. Park, K. Jung, and J. Choi, "A compact low-cost wideband shielded-loop probe with enhanced performance for magnetic near-field measurements," *IEEE Trans. Electromagn. Compat.*, Vol. 62, No. 5, 1921–1928, 2020.
15. Kanda, M., "Standard probes for electromagnetic field measurements," *IEEE Trans. Antennas Propag.*, Vol. 41, No. 10, 1349–364, 1993.
16. Dimitrijević, T., A. Atanaskovic, N. S. Dončov, D. W. P. Thomas, C. Smartt, and M. H. Baharuddin, "Calibration of the loop probe for the near-field measurement," *International Journal of Microwave and Wireless Technologies*, Vol. 12, No. 9, 878–884, 2020.
17. Choi, G. R. and H. H. Park, "Analytical probe factor models for rectangular loop probes used in near-field measurements," *IEEE Trans. Electromagn. Compat.*, Vol. 63, No. 6, 1781–1790, 2021.
18. Oganezova, I., R. Kado, B. Khvitia, Z. Kuchadze, A. Gheonjian, and R. Jobava, "EMC model of low voltage DC motor," *2014 IEEE International Symposium on Electromagnetic Compatibility*, Raleigh, US, November 2014.